Experimental investigation of the impact of macroalgal mats on the wave and current dynamics

N. Tambroni[a,*], J. Figueredo da Silva[b], R. W. Duck[c], S. J. McLelland[d], C. Venier[e], S. Lanzoni[e]

[a]*Dept. of Civil, Environmental and Architectural Engineering, University of Genoa, Genoa, Italy*
[b]*Departmento de Ambiente e Ordenamento, University of Aveiro, 3810-193 Aveiro, Portugal*
[c]*School of the Environment, University of Dundee, Dundee DDI 4HN, United Kingdom*
[d]*Department of Geography, University of Hull, Hull HU6 7RX, United Kingdom*
[e]*Dept. of Civil, Architectural and Environmental Engineering, University of Padua, 35131 Padua, Italy*

Abstract

Macroalgal mats of *Ulva intestinalis* are becoming increasingly common in many coastal and estuarine intertidal habitats, thus it is important to determine whether they increase flow resistance, promote bed stability and therefore reduce the risk of erosion favoring tidal flooding or degradation of coastal lagoons. Venier et al. (2012) studied the impact of macroalgal mats of *Ulva intestinalis* on flow dynamics and sediment stability for uniform flow. Here we extend their experimental work to the case of vegetation under the combined action of waves and currents. These hydrodynamic conditions are very common in many shallow coastal environments and lagoons. The experimental facility employed in the present study and the series of flow runs are the same as that used by Venier et al. (2012). However, waves have been superposed to uniform current flowing firstly over a mobile sediment bed covered with *U. intestinalis*, then over a bare sediment surface. For the depth, wave and current conditions considered in the experiments, the time-averaged vertical profile of horizontal velocity for the case of coexisting waves and current turns out to be very close to that observed for a pure current, both with and without vegetation. However, contrary

*Corresponding author
Email address: nicoletta.tambroni@unige.it (N. Tambroni)

to what was observed in the case of a unidirectional current, in the presence of waves the time averaged velocity profile is only weakly influenced by the vegetation, whose main effect is to attenuate velocity oscillations induced by waves and to slightly increase the overall bed roughness.
Keywords: Ulva intestinalis, wave-current interaction, shear stresses, sediment transport

1. Introduction

Due to the observed increase of macroalgal mats in many coastal and estuarine intertidal habitats [Bolam et al. (2000), Silva et al. (2004)], the scientific community has been recently tasked with improving the present state of knowledge on role of macroalgae in shallow coastal ecosystems. From a hydrodynamical and morphodynamical point of view the issue has recently been addressed by Venier et al. (2012). This experimental study provided an overview of how *Ulva intestinalis* affects unidirectional flow over a sandy bed. The data collected for a range of flow depths that is typical of tidal environments suggest that macroalgae exert a significant stabilizing effect even when the algal cover is sparse. As documented by direct observations and bed elevation measurements, and unlike most of the plants used in other laboratory flume studies [**Augustin et al. (2009), Bouma et al. (2009)**], this species of macroalgae tend to lie flat over the bed, moving sinusoidally with the current. The interaction of the macroalgae with the flow results in a decreased bedform amplitude, with small bedforms forming around the macroalgae strands. In other words, *Ulva intestinalis* provides shelter to sediment grains on the bed, changing the morphology and migration rate of bedforms. Moreover, the interaction of the fronds and bedforms results in an upward shift of the roughness sublayer, where shear stress is more intense. The resulting vertical distributions of the longitudinal velocity and of shear stress suggest that macroalgae lead to a decrease of the near bed mean velocity and an increase of the overall flow resistance. The total friction velocity is generally greater over macroalgae than over bare bed.

The presence of macroalgae, however, also contributes to a reduction in the effective bed shear stress associated with skin friction, responsible for sediment motion. The overall sediment mobility, and hence the amount of transported sediment, are thus reduced. Note that the study of Venier et al. (2012) focused on macroalgal mat interactions with steady unidirectional flow conditions. Nevertheless, both temporal and spatial flow dynamics are crucial to fully understand the momentum transfer mechanisms and their influence on flow resistance [Nikora et al. (2001), Nikora et al. (2004)]. Here, we complement the above analyses by assessing the influence of macroalgal mats on sediment transport in wave-current induced flows. Most of previous studies, conducted in the field or in the laboratory to understand the interaction between hydrodynamics and vegetation, considered the case of flow driven by an uniform current or by regular waves [e.g., Stratigaki et al. (2011), Asano et al. (1998), Romano et al. (2003), Stephan and Gutknecht (2002), Wang et al. (2009), Ghisalberti and Nepf (2004)]. Few observations have been performed including both the effects of currents and waves over a vegetated bottom [Paul et al. (2010), Hu et al. (2014)].

On the other hand, many efforts have been carried out by the scientific community with the purpose of analyzing wave-current non linear interactions in the simplest case of an unvegetated bottom. Laboratory experiments [Kemp and Simons (1982), Kemp and Simons (1983), Visser (1986), Klopman (1994), Klopman (1997), Umeyama (2005); Musumeci et al. (2006); Simons et al. (1996) among others] showed that when waves and currents coexist, the steady profile of longitudinal velocity changes the logarithmic shape observed for pure current conditions. In particular, Kemp and Simons (1982) showed that mean longitudinal velocities close to a smooth bed increase in the presence of waves, whereas they reduce near a rough bed. Furthermore, when waves propagate in an opposite direction with respect to the current, the longitudinal current intensity reduces near to the bed. Musumeci et al. (2006) showed that if the bed is smooth, an increase of the near bottom velocities occurs when waves are perpendicular to the current. The opposite happens when the bottom is rough. Moreover, observed current profiles suggest that wave-current interaction ef-

fects are not restricted to the near bottom region, but influence the entire water column [Kemp and Simons (1982), Kemp and Simons (1983), Klopman (1994), Umeyama (2005)]. These effects mainly depend on the propagation directions of waves and currents. While for parallel and perpendicular cases a reduction of the current intensity is observed in the region below the wave trough, the contrary occurs for opposing waves and currents. As suggested by Kemp and Simons (1983), variations of steady current profile also depend on wave amplitude and on water depth. In addition to experimental studies, various analytical and numerical models have been developed to describe the bottom boundary layer flow under waves and currents. Here we mention the models of Grant and Madsen (1979), Fredsoe (1984) and Davies et al. (1988). We refer the interested reader to Olabarrieta et al. (2010) and Tambroni et al. (2015) for an overview of more recent contributions to the mathematical study of wave-current interactions.

The combination of wave characteristics and current speed investigated here, are those typically found in intertidal areas, supporting macroalgae growth within coastal lagoons dominated by tidal action. In particular, we focus on flow fields that are characterised by relatively low values of the ratio between the amplitude of horizontal orbital velocity and the current velocity (i.e., strong current - weak wave). The main aim of this paper is to compare the behaviors of a bare sediment bottom and of a sediment bottom covered by macroalgae under the combined action of waves and currents through the analysis of the vertical distribution of stationary velocity profiles and turbulent Reynolds stresses.

The body of the paper is organised as follows. In Section 2 we briefly describe the experimental apparatus and the test configuration. Section 3 is devoted to the analysis of velocity data collected in the tests, with particular reference to the characteristics of turbulence observed with and without waves. Finally, Section 4 reports some conclusions and suggestions for future research.

2. Materials and methods

2.1. Experimental facility

Experiments were carried out in the Total Environment Simulator (TES) recirculating flume at the University of Hull (UK), equipped both with pumps to generate flow and paddles to generate waves. The experimental facility is the same described in detail by Venier et al. (2012), therefore we will just briefly summarise the main characteristics of the experimental setup. Length and width of the flume tank were 11 m and 2 m, respectively. Experiments were conducted over a mobile bed, with and without vegetation, in the presence of both waves and currents. In particular, sediment chosen for the experiments was a non-cohesive, unimodal and well-sorted fine sand, characterized by a median grain size of 0.135 mm, which is similar to that of the sediments covering the tidal flats of Budle Bay (NE, England), where strands of *Ulva intestinalis* were collected for the present tests. This is a common macroalga which can be very abundant in nutrient enriched coastal systems. The algae was planted, following the regular pattern shown in Figure 1, in a 20 cm thick sediment bed that was leveled before the start of the experiments. The density of the plantings (12 plants per m^2) intended to represent a sparse algal mat cover (~ 30 %) and was characterised by a lateral and longitudinal spacing equal to 20 cm and 40 cm, respectively. The large number of fronds attached to each strand generated a fan shape covering up to 20 by 10 cm of the sandy bed.

Velocity measurements were collected in a 2 m wide and 2 m long sampling volume placed approximately at the centre of the flume [see Figure 1 of Venier et al. (2012)]. This measuring area was located 6 m downstream of the flume inlet, to ensure fully developed, uniform flow conditions and to enable wave form development. The longitudinal, lateral and vertical velocity components, (u_x, u_y, u_z), were measured at a set of selected points by means of four Nortek laboratory ADVs, denoted as ADV0, ADV1, ADV2, ADV3 in Figure 2. These devices were located 1.2, 1.1, 1.0 and 0.9 m from the flume wall and were moved longitudinally to monitor the along-flow positions X1, X2, X3, X4 lo-

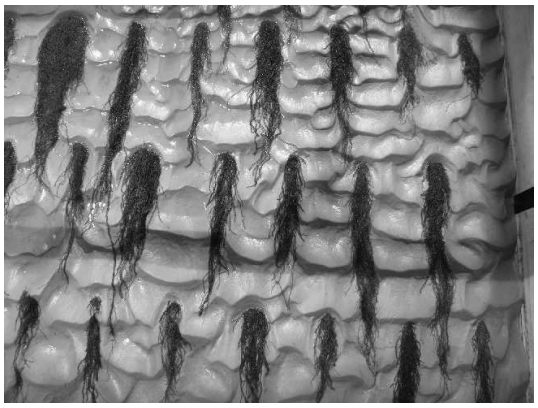

Figure 1: Example of the typical bed pattern observed in the present experiments.

cated 0.8, 1.0, 1.2 and 1.4 m from the upstream limit of the measuring area. Up to 10 different points, depending on the flow depth, were sampled at each given vertical and velocities were sampled at a frequency of 25 Hz for an acquisition time of 120 s. The ADV sampling volume was approximately 350 mm^3.

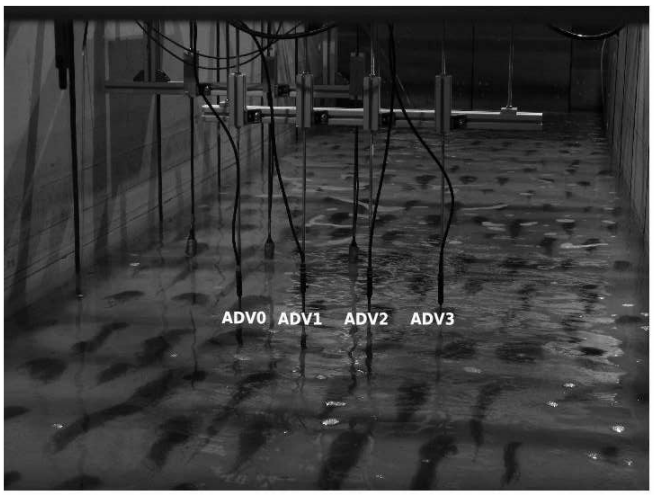

Figure 2: Picture of the measuring area

The total mass of sediment transported along the flume as bedload was measured at the end of each run by weighing sediment collected within a series

of pit-type traps located across the downstream end of the flume.

2.2. Experimental programme

As reported in Table 1, the experimental programme involved three runs (hereafter denoted by the subscript 'wc' to indicate the combined wave-current conditions) conducted for three different water depths in the presence of both a unidirectional flow and a monochromatic, regular train of waves. The water depths and pumping discharges imposed in the experiments were selected in order to ensure the same mean flow conditions employed in the experiments of Venier et al. (2012), typical of micro-tidal environments. The wave height and period were chosen to represent fully developed wind wave conditions for each of the considered water depth. For comparison, Table 1 includes also data in the previous set of experiments performed by Venier et al. (2012) under unidirectional flow conditions. We will refer to this latter set of experiments using the same notation, with the only difference that the subscript 'c' will be used to denote pure current conditions in the absence of waves.

A first series of experiments (denoted as M) were conducted with the sandy bed covered with *Ulva intestinalis* and salt water (density $\rho = 1027\ kg/m^3$). The macroalgae were then removed from the flume, the salt water was replaced with fresh water (ρ=999 kg/m^3) and, after flattening the bed, a second series of tests (denoted as B) was carried out under the same initial hydraulic conditions of the M runs. The experiments were run for the minimum time needed to develop stable bedforms along the flume, before beginning measurements.

3. Data analysis

The Acustic Doppler Velocimeter (ADV) time series were firstly filtered, removing erroneous values and correcting for tilt and misalignment of the probes. In particular, the data removed consisted of i) measurements closer than 0.5 cm to the bed and ii) measurements containing more than 5% of bad data, namely points for which the mean and the minimum correlation were < 70 and < 50,

Table 1: Summary of the experimental tests, carried out for three different water depths under either unidirectional current (subscript c) (Venier et al. 2012) or waves superposed to a uniform flow (subscript wc), and a sandy bed either bare (B tests) or covered with macro algae (M tests). Notations are as follows: D: depth of the still water initially filling the flume; Q: water discharge used to obtain a uniform unidirectional flow; H_w: wave height; T_w: wave amplitude; L_{th}: wave length according to the dispersion relation provided by the linear Stokes theory; U_x: depth averaged value of the spatially and time averaged longitudinal velocity; L_{bf}: observed bedform wavelength; Q_s: measured mass sediment flow rate per unit width transported as bedload.

Run	$M1_c$	$M1_{wc}$	$M2_c$	$M2_{wc}$	$M3_c$	$M3_{wc}$	Bed
	$B1_c$	$B1_{wc}$	$B2_c$	$B2_{wc}$	$B3_c$	$B3_{wc}$	
D (m)	0.22	0.22	0.25	0.25	0.31	0.31	
Q (ls^{-1})	90	90	102	102	124	124	
H_w (m)	-	0.09	-	0.10	-	0.12	
T_w (s)	-	1.0	-	1.0	-	1.1	
L^{th} (m)	-	1.25	-	1.30	-	1.60	
U_x	0.22	0.24	0.26	0.254	0.26	0.23	M
(ms^{-1})	0.23	0.26	0.28	0.23	0.27	0.27	B
L_{bf}	10.4	6.6	11.7	6.8	10.2	6.8	M
(cm)	9.8	7.3	/	8.2	12.4	8.5	B
Q_s	-	8.11	0.60	13.00	0.06	9.80	M
$(10^{-4}$ $kgm^{-1}s^{-1})$	0.67	9.90	/	12.00	0.50	12.0	B

while the mean and the minimum signal to noise ratio (SNR) were < 15 and < 5, respectively. A detection routine was used to remove high velocity spikes from the time series. The corrections for probe tilt and misalignment involved rotating the velocity vectors in the horizontal and vertical planes such that the average lateral and vertical velocities within the entire fluid volume spanned by ADV measurements were zero (thus ensuring one dimensional bulk flow conditions). Generally, the tilt and misalignment correction angles were so small as to render the corresponding corrections negligible. After these preliminary operations, the time averaged velocity vector $\vec{\bar{u}}$ was calculated at each sampling point, by averaging over the total acquisition time. The instantaneous velocity vector $\vec{u}$ was then decomposed as:

$$\vec{u} = \vec{\bar{u}} + \vec{\tilde{u}} + \vec{u}' \tag{1}$$

where $\vec{u}'$ is the vector of the turbulent velocity fluctuations and $\vec{\tilde{u}}$ is the wave induced orbital velocity. The wave induced velocity possesses a periodic nature and may be determined by phase-averaging the instantaneous velocity, detrended by the time average $\vec{\bar{u}}$:

$$\vec{\tilde{u}} = \lim_{N\to\infty} \frac{1}{N} \sum_{n=0}^{N} [\vec{u}(t + nT) - \vec{\bar{u}}] \tag{2}$$

where T is the wave period, n is the number of the wave cycle and N the total number of wave cycles.

Before analysing in detail the specific features emerging from the temporal and spatial distributions of $\vec{u}$, it is worthwhile discussing the overall structure of the sediment bed resulting from direct observations. In all the experiments, the bed was rapidly covered by bedforms with sinuous crest-lines (Figure 1). As reported in Table 1, in the experiments characterised by the presence of both waves and currents, bedforms were generally shorter (wavelength L_{bf} in the range 6.6-8.5 cm) than in the pure current case (L_{bf} in the range 9.8-12.4 cm). In the presence of *Ulva intestinalis* the flow meandered around the algal strands, generating slightly smaller linguoid bedforms, migrating around the points of

attachment of the algal strands (see Figure 1). In some cases bedform migration caused a partial burial of algal strands. Visual observations also highlighted that algal filaments oscillated sinusoidally both in the lateral and vertical directions, with the meandering of near bed flow. This behaviour was observed both in the presence and in absence of waves and is very different from that of the majority of plants analysed in laboratory experiments, in which the vegetation occupied a significant portion of the water column [**Shi et al. (1995), Augustin et al. (2009)**].

3.0.1. Vertical distribution of the longitudinal velocity

The first analysis carried out on the velocity data concerned the vertical distribution of the stationary (i.e., averaged over the total sampling time) component of the longitudinal velocity, $\bar{u}_x$.

First of all, it was preliminary verified that the vertical $\bar{u}_x$ profile does not undergo any significant change in the direction of motion. To verify this, for each experiment in the presence of waves, a graph has been constructed comparing the vertical profiles of $\bar{u}_x$, averaged laterally, $\langle \bar{u}_x \rangle$ (hereafter $\langle \ldots \rangle$ will denote lateral averaging), and measured at different locations along the flow direction, x. Figure 3 shows that the variations between these profiles are very small.

In order to obtain a macroscopic description of the flow features within the study area, the vertical profiles of the stationary longitudinal velocity have been averaged laterally and along x (we will denote by $\langle\langle \bar{u}_x \rangle\rangle$ this spatial double averaging in horizontal planes parallel to the bed). Each plot of Figure 4 shows a comparison between the dimensionless double averaged stationary velocity profiles observed with and without waves.

It should be noted, when interpreting the results, that both waves and currents propagate in the positive x direction. Previous experiments considering combined waves-current motion [see, among others, Kemp and Simons (1982), Kemp and Simons (1983), Klopman (1994), Klopman (1997), Umeyama (2005)], show that the vertical profile of the stationary component of the longitudinal velocity experiences a significant reduction near the free surface when the waves

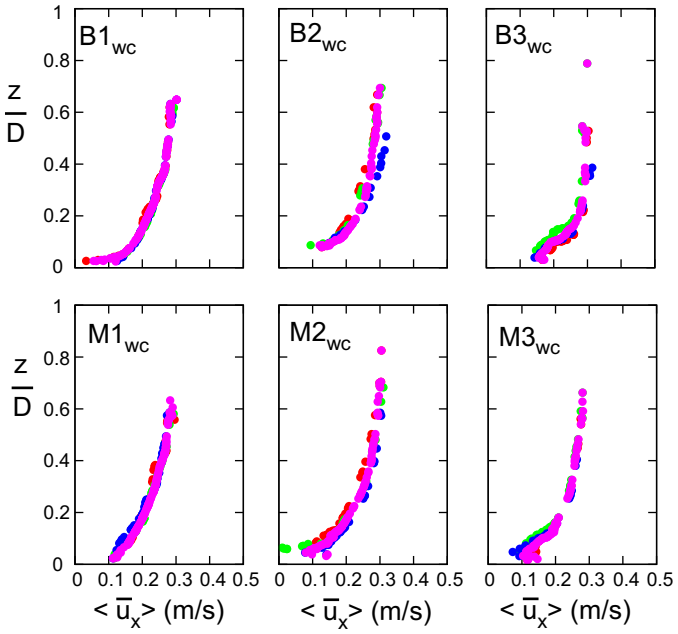

Figure 3: Vertical profiles of the stationary (averaged over the total sampling time) component of the longitudinal velocity, averaged laterally, $\langle \bar{u}_x \rangle$, and measured at different locations X_i along the flow direction, in the presence of waves superposed to a unidirectional uniform flow. The elevation with respect to the initial flat bed, z, has been normalised by the mean flow depth D. Symbols are as follows: blue circles, $X_2 = 100\ cm$; green circles, $X_3 = 120\ cm$; red circles, $X_4 = 140\ cm$; magenta: along x average value.

propagate in the same direction of the current, and an increase of the current velocity near the free surface when the waves propagate in the opposite direction. In particular, the experiments of Umeyama (2005) suggest that when waves and currents propagate in the same direction, a local maximum of the longitudinal velocity $\bar{u}_x$, exits at an elevation of roughly 0.5 times the mean water depth from the bottom for wave periods of roughly 1 s, and that an increase in the wave period lowers this point of maximum.

Comparison reported in Figure 4 suggests that in the present experiments waves weakly influence the shape of the mean current profile. The lack of data in the upper region of the water column, due to the intrinsic limitations of ADV measurements, makes it difficult to detect the typical reduction of the current

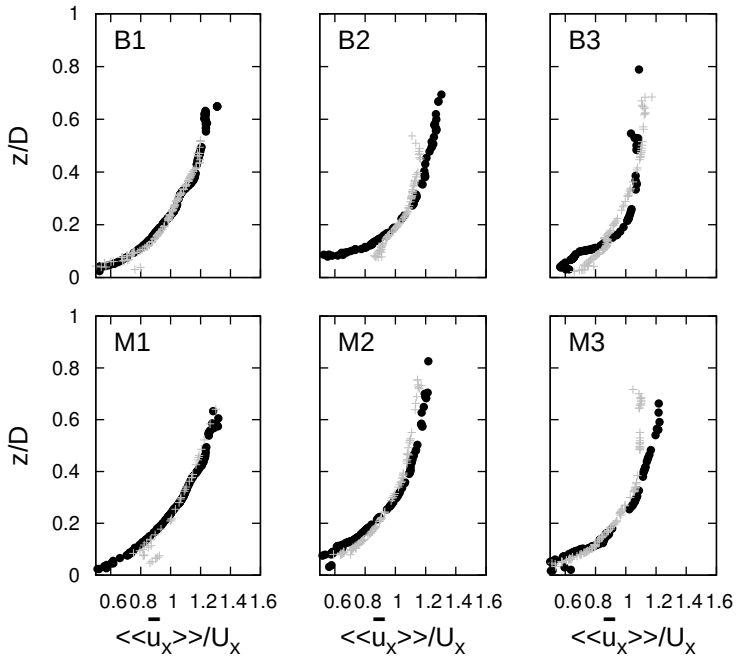

Figure 4: Upper plots: spatially and laterally averaged profiles of the time averaged longitudinal velocity $\bar{u}_x$ for the non-vegetated experiments (B). Lower plots: spatially and laterally averaged profiles of the time averaged longitudinal velocity $\bar{u}_x$ for the vegetated case (M). The dimensionless comparison is produced for the vertical coordinate by scaling z with the flow depth while the double averaged longitudinal velocity, $\langle\langle\bar{u}_x\rangle\rangle$, has been normalized with its depth averaged value, U_x. The values assumed by U_x for the different experiments are reported in Table 1. Crosses indicate pure current experiments (c) and dots indicate waves plus current experiments (wc).

velocity near the free surface, as observed by Umeyama (2005). In any case it is worth comparing the observed $\langle\langle\bar{u}_x\rangle\rangle$ profiles with the typical logarithmic profile which better fits the experimental data.

Figure 5 indicates that the steady component of the longitudinal velocity begins to slightly deviate from the logarithmic law at approximately 50% of the mean water depth above the bed. The presence of a local maximum in the velocity profile is more evident in experiment $B3_{wc}$, which is characterized by greater flow depth and wave period. Similar to observations made by Umeyama

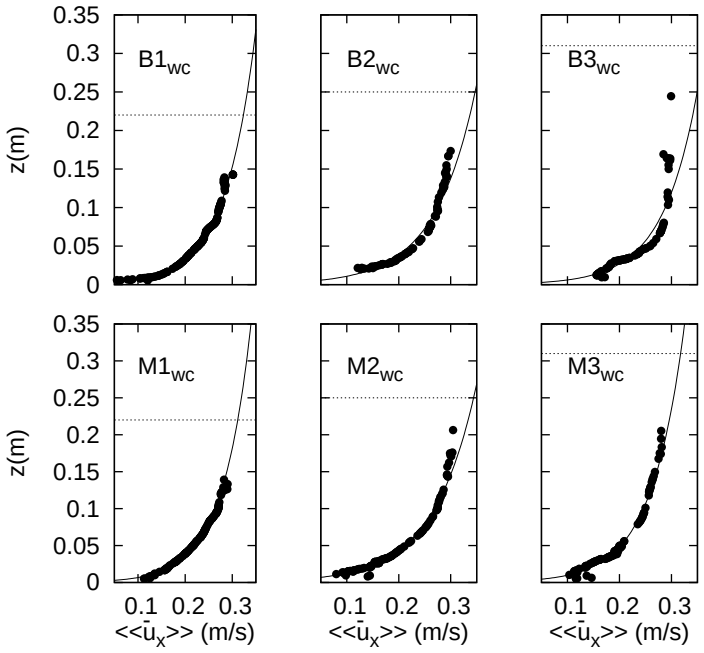

Figure 5: Comparison between the vertical distribution of the stationary current profile $\langle\langle \bar{u}_x \rangle\rangle$ measured in the experiments with waves and currents (dots) and logarithmic velocity profile (line) which better fits the data. Horizontal dotted lines denote the position of the mean free surface elevation, the values of the mean flow depth are 0.22, 0.25 and 0.31 m in experiments B/M1, B/M2 and B/M3, respectively.

(2005), in experiments $B1_{wc}$ and $B2_{wc}$, the point of velocity maximum likely occurs at a higher elevation above the bed, since in these experiments the wave period is smaller than in experiment $B3_{wc}$. Comparison with the profiles observed in experiment $B3_{wc}$ and $M3_{wc}$ suggests that the presence of vegetation may cause an increase in the height of the local maximum of the velocity profile.

The weak influence of the waves on the stationary velocity profiles characterizing the present experiments can also be explained by the fact that non-linear effects arising from wave and current interaction are only evident if the wave component and the current component are comparable in magnitude. However, comparison between the results shown in Figures 3 and 6 suggests that in the present experiments the current velocity (Figure 3) is almost twice the amplitude of the velocity oscillations induced by wave propagation (Figure 6). Therefore, the waves are too weak or the currents are too strong to enable the nonlinear effects to become dominant. Hence, under the condition of a weaker current or stronger waves, not covered in the present experiments, the wave effect may become more apparent and the computed time-averaged vertical profile may more clearly deviate from that for pure current, in accordance with the observations of Umeyama (2005). Note that the ratio between the amplitude of the velocity oscillations induced by wave propagation and the current velocity investigated by Umeyama (2005) is in the range 0.7-0.87 and, hence, typically 50% greater than the ratio employed in our experiments. From this analysis it is not surprisingly that the effect of waves is more evident in experiment $B3_{wc}$ which is characterized by the higher amplitudes of the velocity oscillations induced by wave propagation.

Figure 6 also suggests that the presence of macroalgae slightly reduces the amplitudes of velocity oscillations induced by waves, further weakening the influence of the waves on the stationary velocity profiles. This result is in agreement with both the physical experiments and numerical simulations of Li and Yan (2007), suggesting that the interaction of waves and current leads to a greater attenuation of waves in the presence of vegetation.

Finally, it must be noted that wave reflection may have partially impacted

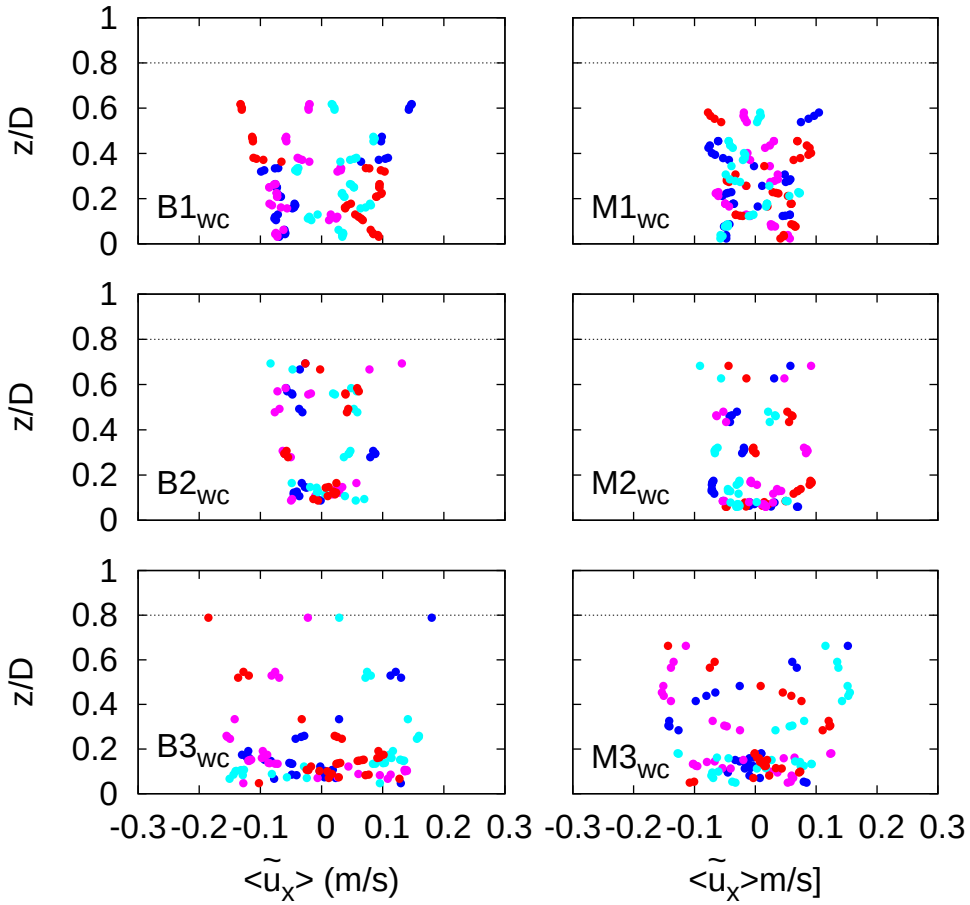

Figure 6: Variation of the vertical profile of laterally and phase averaged wave induced velocity $< \tilde{u}_x >$ at the position X_3 for different phases of the wave cycle: $t = 0$, blue circles; $t = T_w/4$, magenta circles; $t = T_w/2$, red circles; $t = 3T_w/4$, cyan circles.

on the observed stationary velocity profiles. In fact, despite the placement of an absorber device at the end section of the experimental flume opposite to that where the waves were generated, owing to the physical constraint of the experimental apparatus, waves were not completely dissipated but underwent a partial, not quantificable reflection at this boundary.

3.0.2. Shear velocity and Nikuradse roughness

It is well known that in fully developed turbulent flows occurring over a rough bed the vertical distribution of $\bar{u}_x$ is well approximated by a logarithmic law of the form:

$$\frac{\bar{u_x}}{u_*} = 5.75 log(\frac{z}{e_s}) + 8.5 \tag{3}$$

where u_* is the friction velocity, e_s is the Nikuradse roughness parameter and z is the elevation over the mean bed surface.

In order to quantify the differences/similarities between the vertical distributions of the time averaged velocity, $\bar{u}_x$, resulting in the cases with and without waves, we have assumed that Eq. 3 also holds in the presence of waves, at least outside the bottom and surface boundary layers. We have thus determined u_* and e_s from Figure 7, plotting the term 5.75 $\log_{10}(z)$ versus the temporally and spatially averaged longitudinal velocity $\langle\langle \bar{u}_x \rangle\rangle$. In particular, a linear fitting of the experimental data has been performed and the correlation coefficient measuring the reliability of the fitting has been estimated. In conditions both with and without waves, the velocity measurements are well represented by Eq. 3, although some larger deviations occur near to the bed and to the free-surface in the presence of waves. The slope m and the intercept b of the straight lines in Figure 7 allow estimation of the friction velocity $u_* = 1/m$ and the roughness coefficient $e_s = 10^{(b+8.5)}/5.75$.

A graphic summary of all the values of u_* and e_s provided by this analysis is reported in Figure 8, while the representative values of these parameters are summarised in Table 2.

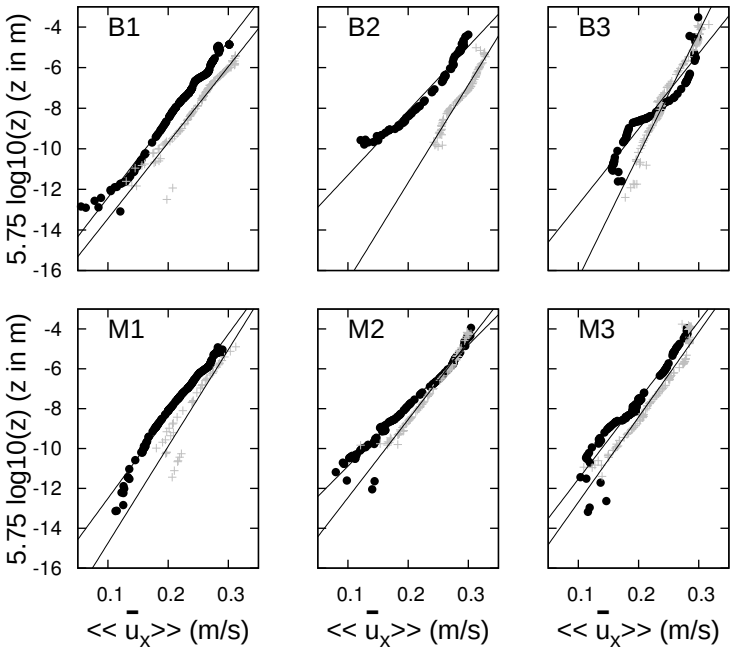

Figure 7: Spatially and time-averaged velocity profiles in a semilogarithmic plane. Upper plots: non-vegetated experiments. Lower plots: vegetated experiments. Crosses refer to uniform flow experiments, while filled circles refer to the waves plus current cases. Solid lines indicate linear interpolation in the semi-log plane.

Table 2: Values of friction velocity, u^*, and of roughness parameter, e_s, resulting from the linear interpolations of Figure 7.

Run	$M1_c$	$M1_{wc}$	$M2_c$	$M2_{wc}$	$M3_c$	$M3_{wc}$	Bed
	$B1_c$	$B1_{wc}$	$B2_c$	$B2_{wc}$	$B3_c$	$B3_{wc}$	
u^*	0.021	0.024	0.026	0.033	0.023	0.025	M
(m/s)	0.027	0.026	0.021	0.032	0.017	0.027	B
e_s	0.012	0.039	0.043	0.114	0.034	0.061	M
(m)	0.031	0.045	0.006	0.092	0.004	0.041	B

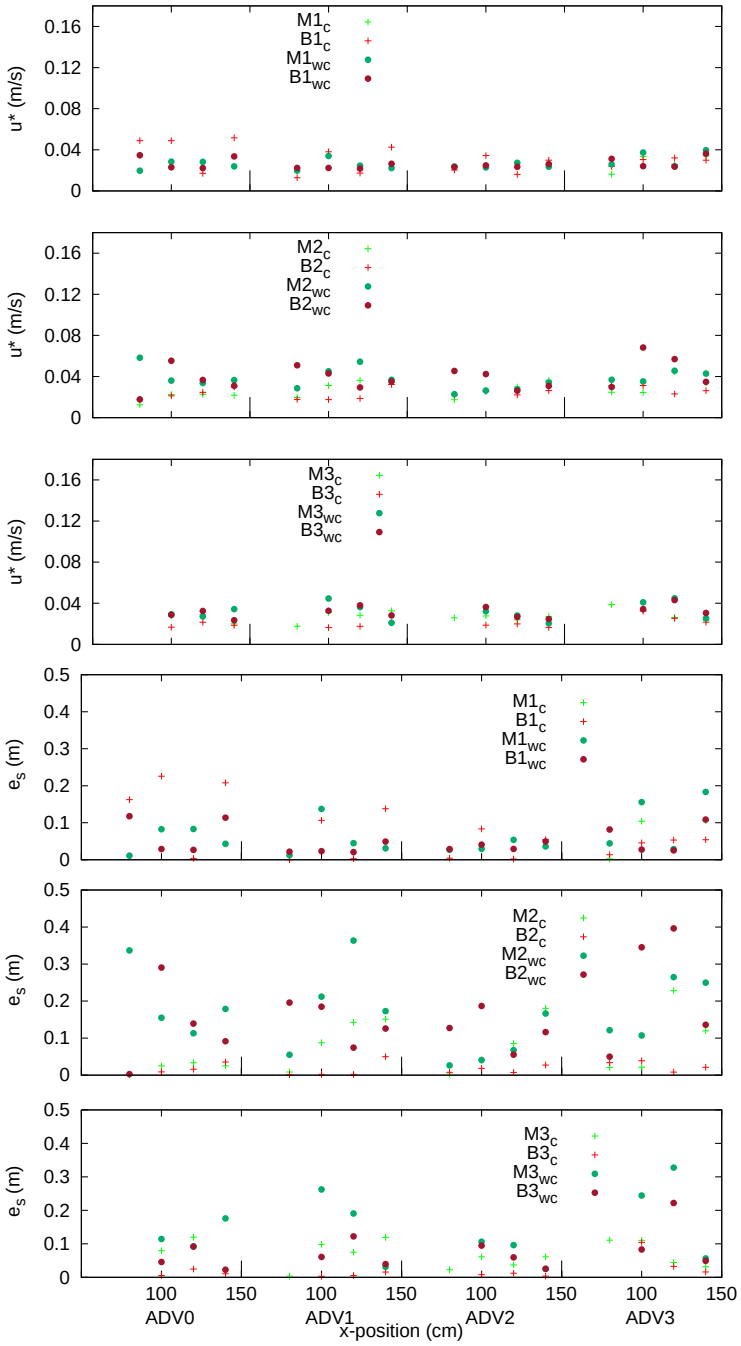

Figure 8: Summary of the friction velocity, u_*, and of the roughness parameter, e_s estimated for the various tests.

It appears that the friction velocity generally attains larger values in the presence of waves than in the unidirectional uniform flow case. This is particularly evident in run 2, where the reference value of u_* of run $B2_{wc}$ is 0.032 m/s, while that referring to experiment $B2_c$ is 0.021 m/s. The influence of waves is even more marked in the case of the roughness parameter. The values of e_s in run $B2_{wc}$ are indeed much greater than those estimated without waves, the reference values in experiments $B2_{wc}$ and $B2_c$ being 0.092 m and 0.006 m, respectively. Run 3 provides analogous results, while for the set of run 1, both friction velocity and roughness parameter attain almost the same values in the absence and in the presence of waves. As far as the effect of the vegetation is concerned, with exception of run 1, the values of e_s in the presence of macroalgae are generally greater than those for a bare bed, although in the presence of waves, the difference between the values of e_s observed with and without macroalgae is smaller. Finally, while in the case of a unidirectional current the friction velocity u_* is on average slightly larger over macroalgae than over bare bed (runs 2 and 3), in the presence of waves, macroalgae do not seem to alter significantly the value of u_* observed over bare bed. Therefore, for the algal mat density considered in the present experiments (reproducing a sparse cover $\sim 30\%$), the global effect on the flow field induced by the superposition of regular waves to a unidirectional current consists only of a moderate increase of the roughness parameter while the friction velocity remains almost unaltered.

Despite its complexity, the problem of wave-current interaction has also been tackled theoretically [see, among others, Grant and Madsen (1979), Fredsoe (1984), Davies et al. (1988), Olabarrieta et al. (2010) and Tambroni et al. (2015)]. The most recent theories appear to provide a reliable description of the flow field not only in the wave-current boundary layer but also along the entire water column. However, these mathematical models still require a numerical solution of the problem and hence, do not entail a straightforward application. For the sake of simplicity, in order to check if our results are consistent with the existing theoretical predictions, the simple approach of Grant and Madsen (1979) has been applied to estimate analytically the values of e_s in the case of coexisting waves

Table 3: Summary of the main experimental parameters, and comparison between the typical roughness values measured in the experiments and the values suggested by the theory of Grant and Madsen (1979). Values of the skin component of the total shear stresses τ_b' have been evaluated from equation (6), while estimate of the mass sediment flow rate per unit width, Q_{scalc}, have been obtained by applying the Meyer-Peter and Muller (1948) formula.

Run	$B1_{wc}$	$M1_{wc}$	$B2_{wc}$	$M2_{wc}$	$B3_{wc}$	$M3_{wc}$
$D\ (m)$	0.22	0.22	0.25	0.25	0.31	0.31
$H_w\ (m)$	0.09	0.09	0.10	0.10	0.12	0.12
$T_w\ (s)$	1.0	1.0	1.0	1.0	1.1	1.1
$u_{*c}\ (ms^{-1})$ exp	0.027	0.021	0.021	0.026	0.017	0.023
$e_{sc}\ (m)$ exp	0.031	0.012	0.006	0.043	0.004	0.034
$e_{swc}\ (m)$exp	0.045	0.039	0.092	0.114	0.041	0.061
$e_{swc}\ (m)$ theory	0.077	0.035	0.024	0.106	0.015	0.084
$\tau_b'\ (Pa)$	0.178	0.165	0.205	0.202	0.211	0.163
$Q_s\ (10^{-4}\ kgm^{-1}s^{-1})$	9.90	8.11	12.00	13.00	12.0	9.80
$Q_{scalc}\ (10^{-4}\ kgm^{-1}s^{-1})$	8.60	6.37	13.47	12.96	14.8	6.12

and currents. The results, shown in Table 3, demonstrate that the roughness values predicted by the theory of Grant and Madsen (1979) reproduce reasonably those resulting from our flume measurements.

3.0.3. Vertical Distribution of Shear Stresses

The vertical distribution of the Reynolds stresses through the flow depth is usually calculated from the values of the measured fluctuating velocities. However, in the presence of waves, the variance associated with waves is often much larger than that associated with turbulence. Some form of wave-turbulence decomposition must then be used. In a flow with both waves and currents, the instantaneous velocity can be decomposed as described by Eq. 1. After averaging the mean momentum equations over the turbulence (Reynolds averaging), the Reynolds stress becomes:

$$-\frac{\tau_t}{\rho} = \overline{\tilde{u}_x \tilde{u}_z} + \overline{\tilde{u}_x u'_z} + \overline{u'_x \tilde{u}_z} + \overline{u'_x u'_z} \tag{4}$$

where u'_x and u'_z are the fluctuating velocity along the longitudinal and the vertical direction, and an overbar denotes turbulence averaging.

For irrotational, progressive waves [Dean and Dalrymple (1991)], the first term on the right hand side (rhs) of equation 4 is zero. Furthermore, when waves and turbulence coexist, the latter is defined as motions that do not correlate with waves [Jiang and Street (1991), Thais and Magnaudet (1995)]. As a consequence, the second and third terms on the rhs of equation 4 are also zero. Under these conditions, the Reynolds stresses take the same form characterizing steady flows:

$$-\frac{\tau_t}{\rho} = \overline{u'_x u'_z} \tag{5}$$

However, as shown by Trowbridge (1998), small uncertainties in instrument orientation or a gently sloping bed can bias velocity measurements such that in practice $\overline{\tilde{u}_x \tilde{u}_z}$ may not be exactly zero. Various methods of wave-turbulence decomposition can be used to remove this wave contamination from a turbulence

dataset. Here we employ the 'phase' method introduced by Bricker and Monismith (2007), where the phase lag between the instantaneous velocity components u_x and u_z of surface waves is used to interpolate the magnitude of turbulence under the wave peak within the inertial subrange of the spectral domain.

Figure 9 reports the resulting vertical profiles of turbulent shear stresses calculated under uniform flow conditions and in the case of combined waves and currents. First of all, it immediately appears that in the presence of waves the turbulent shear stresses are more intense and attain a maximum at a higher elevation from the bed with respect to the uniform flow case. Similar to the analysis of the mean velocity profiles, the shear stress profiles have been also spatially averaged in horizontal planes parallel to the bed. The resulting profiles are reported in Figure 10. The plots confirm that, as expected, shear stresses are enhanced by the presence of waves. Some peculiar results, however, arise in experiment 3, where, as the elevation above the bed increases, the wave-current Reynolds stresses decrease more rapidly than in the other experiments and change sign, becoming negative at $z >\sim 0.05$. Similar profiles have been observed by Umeyama (2005) in the case of waves following a current. Umeyama (2005) also found that the elevation characterized by vanishing Reynolds stresses decreases as the amplitude of the wave induced velocity oscillations increases. Hence, as already discussed when analysing the spatially averaged stationary velocity profiles, it is possible that in runs 1 and 2 the intensity of the wave induced velocity is too small to allow nonlinear effects due to wave-current interaction to become significant and, consequently, shear stresses do not become negative. Finally, note that the presence of macroalgae lying nearly parallel to the bed and oscillating with the flow does not seem to significantly alter the distribution of turbulent Reynolds stresses both in the presence and in the absence of waves. Nevertheless, macroalgal mats invariably reduce the near bed peak of the turbulent shear stress, while the overall bed shear stress acting just above the narrow layer occupied by macroalgae tends to increase, owing to the form drag related to the presence of both vegetation and bedforms.

In conclusion, despite the formation of shorter bedforms, in the experiments

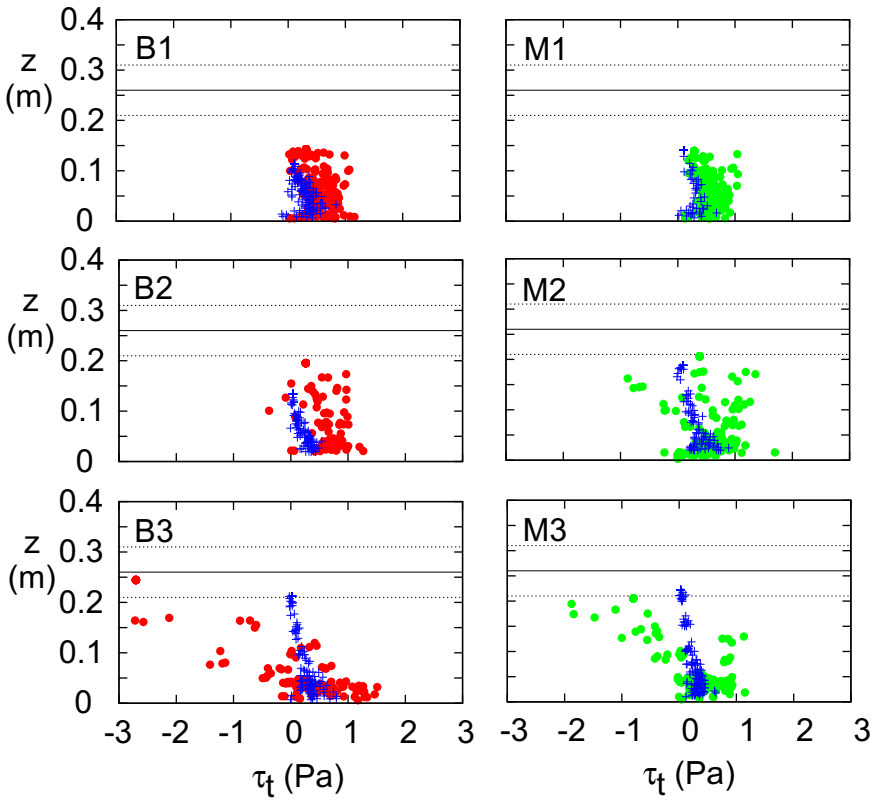

Figure 9: Vertical profiles of turbulent Reynolds stresses, $\tau_t = -\rho\overline{u'_z u'_x}$ for the ADV measurements carried out in: *upper plots*) experiments 1, *middle plots*) experiments 2 and *lower plots*) experiments 3. Crosses identify the experiments carried out with unidirectional flow conditions (Venier et al., 2012); red circles and green circles refer to bare and vegetated bed, respectively, under the action of both waves and an unidirectional current.

with waves it has been observed an increase of the bed shear stresses associated with skin roughness, and consequently a significant (one-two orders of magnitude) increase of the intensity of the sediment transport rate (see Table 1). On the contrary, although to a lesser extent with respect to the case of unidirectional flow conditions, the presence of a sparse macroalgae cover contributes to a reduction in the effective bed shear stress associated with grain roughness responsible for sediment motion.

These findings are supported by the estimates of sediment transport reported in Table 3 and obtained by using the classic Meyer-Peter and Muller (1948) bedload formula. For a steady current, the skin component, τ_b', (i.e., related to grain roughness) of the total shear stresses suggested by Meyer-Peter and Muller (1948) to be used in the bedload formula is the following:

$$\tau_b' = \mu \tau_b \qquad \mu = \left(\frac{C}{C'}\right)^{1.5} \tag{6}$$

where τ_b is the total shear stress, μ is a bed form factor, C and C' are the overall and grain-related Chezy coefficient, respectively. Note that in the presence of vegetation the values of the skin component of the total shear stresses are typically smaller than for a bare bottom.

The estimated sediment transport rates, reported in Table 3, are quite close to those measured in the experiments. Overall, under the combined action of current and waves, the skin friction and amount of transported sediment turn out to be reduced by the presence of a sparse algal cover, at least for the range of hydrodynamic conditions here investigated. **Hence, by reducing the rate of the sediment erosion, algal mats may significantly influence the morphodynamic behavior of a given coastal wetland. These results suggest that Algal mats (in the present case *Ulva Intestinalis*) basically act as ecosystem-engineer organisms [Jones et al. (1994)] which contribute to modify and to help the maintenance of the habitat they live.**

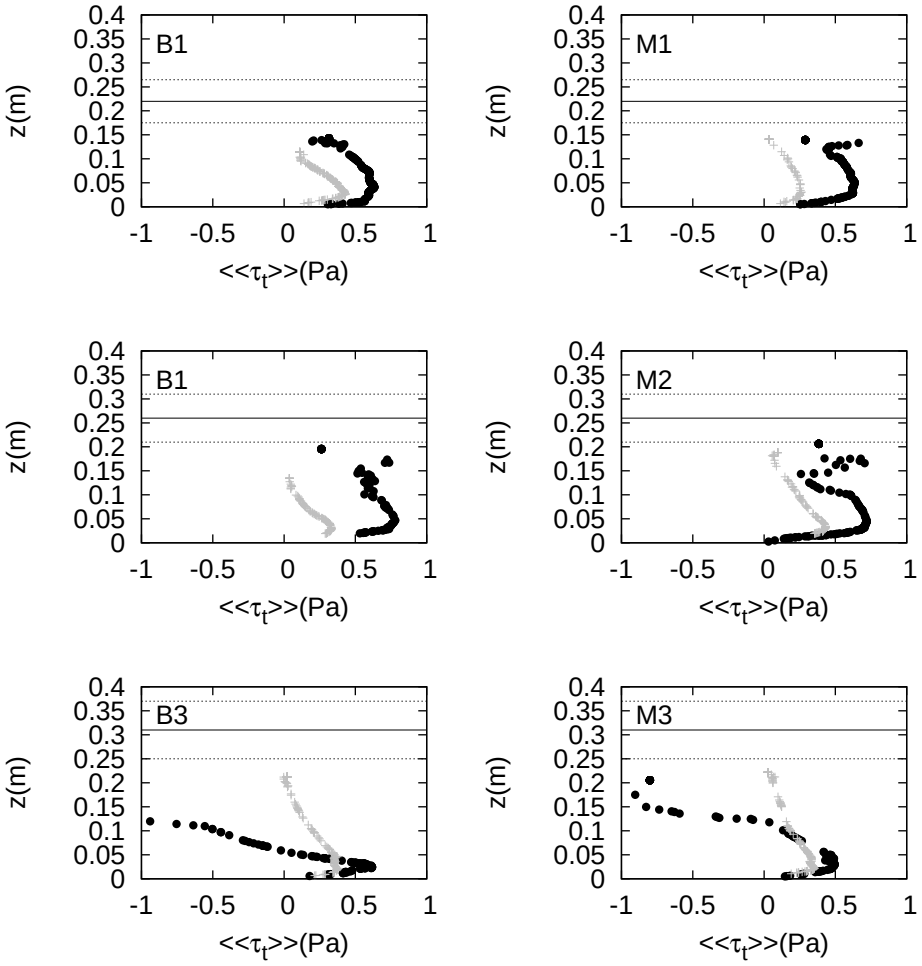

Figure 10: Spatial average over planes parallel to the bed of the turbulent Reynolds stresses, $<< \tau_t >> = -\rho << \overline{u'_z u'_x} >>$ for the ADV measurements carried out in: *upper plots*) experiments 1, *middle plots*) experiments 2 and *lower plots*) experiments 3. Grey crosses identify the experiments carried out with unidirectional flow conditions (Venier et al., 2012); black circles refer to bare and vegetated bed, respectively, under the action of both waves and an unidirectional current.

4. Conclusion

The results of the present research can be summarized as follows.

1. When relatively weak waves are superposed with a strong unidirectional current, as investigated here, the time-averaged vertical profile of horizontal velocity is very close to that observed in the presence of a purely unidirectional current;
2. In the presence of a non-vegetated bed, the global effect of waves on the stationary velocity profile consists of a slight increase of friction velocity and a more significant increase of the corresponding roughness parameter;
3. In the case of waves combined with currents over macroalgae (*Ulva Intestinalis*), the most significant effect of an algal mat is to damp velocity oscillations induced by waves, while the friction velocity remains essentially unchanged and the roughness parameter tends to increase slightly;
4. The presence of waves implies more intense turbulent shear stresses, which attain a maximum at an higher elevation from the bed with respect to pure uniform flow conditions;
5. In the experiment characterized by the higher value of the ratio between the amplitude of horizontal orbital velocity and the current velocity (Run 3), moving away from the bed, the wave-current Reynolds stresses change sign, becoming negative and displaying the typical behavior observed by Umeyama (2005) in the case of waves traveling in the same direction as the current;
6. The presence of macroalgae lying nearly parallel to the bed in the case of a unidirectional flow and waves superposed to a uniform current, does not seem to significantly alter distribution of turbulent Reynolds stresses along the flow depth; nevertheless, macroalgal mats are found to slightly reduce the near bed peak of the turbulent shear stress.
7. The presence of macroalgae generally tends to reduce the effective bed shear stress associated with grain roughness responsible for sediment motion. As a consequence, the amount of sediment transported under the

combined action of current and waves turn out to be reduced even in the presence of a sparse ($\sim$ 30%) algal cover, at least for the range of hydrodynamic conditions here investigated.

Algal mats thus act as ecosystem-engineer organisms [Jones et al. (1994)] that alter the local hydrodynamics near the bottom, affect the rate at which sediment are eroded and, hence, contribute to affect the overall morphodynamic behavior of a given coastal wetland. Algal filaments, aligned nearly horizontally in a narrow layer close to the bed, provide sheltering for sediment from direct flow drag exerted by the combined action of waves and currents. For hydraulic conditions (flow depth and velocity) typical of those encountered in tidal environments under ordinary weather conditions, and realistic macroalgal features (length and width of each individual) this dynamic behaviour has significant consequences even in the presence of a relatively sparse ($\sim$ 30%) algal mat cover. As algal density increases, the sheltering action produced by the algal cover likely leads to a stronger stabilization of the bed [Romano et al. (2003)].

Quantitative scenarios of the response of estuarine environments to both climate changes (e.g., sea level rise, changes in storminess) and planned human interventions (e.g., creation of new defence schemes, either engineered, ecosystem based or hybrid) then require a coupled description of morphodynamic processes and of the feedbacks with biotic communities therein. The present study can help in developing subgrid models (i.e., at a scale smaller that that of the computational grid) describing these feedbacks. To this aim further experimental work is surely needed to assess how sediment transport rates are affected by macroalgal density and by a flow field with higher amplitudes of the horizontal orbital velocity with respect to the current velocity.

5. Acknowlegments

We gratefully acknowledge the important contribution of Brendan Murphy during the experimental stage of this project. This work has been supported by the European Community Sixth Framework Programme through the grant

of the Integrated Infrastructure Initiative HYDRALAB III within the Transnational Access Activities, Contract no. 022441. Partial funding has been also provided by University of Padua within the project (CPDA103051) "Morphodynamics of marsh systems subject to natural forcing and climate changes".

References

Asano, T., Tsutsui, S., Sakai, T., 1998. Wave damping characteristics due to seeweed. Proceedings of 25th Coastal Engineering Conference in Japan , 138–142.

Augustin, L.N., Irish, J.L., Lynett, P., 2009. Laboratory and numerical studies of wave damping by emergent and near - emergent wetland vegetation. Coastal Engineering 56, 332 – 340. doi:10.1016/j.coastaleng.2008.09.004.

Bolam, S.G., Fernandes, T.F., Read, P., Raffaelli, D., 2000. Effects of macroalgal mats on intertidal sandflats: an experimental study. Journal of Experimental Marine Biology and Ecology 249, 123–137.

Bouma, T.J., Friedrichs, M., Van Wesenbeeck, B.K., Temmerman, S., Graf, G., Herman, P.M.J., 2009. Density - dependent linkage of scale - dependent feedbacks: a flume study on the intertidal macrophyte spartina anglica. Oikos 118, 260–268. doi:10.1111/j.1600-0706.2008.16892.x.

Bricker, J.D., Monismith, S.G., 2007. Spectral waveturbulence decomposition. Journal of Atmospheric and Oceanic Technology 24, 1479–1487. doi:10.1175/JTECH2066.1.

Davies, A.G., Soulsby, R.L., King, H., 1988. A numerical model of combined wave and current bottom boundary layer. Journal of Geophysical Research 93(C1), 491–508.

Dean, R.G., Dalrymple, R.A., 1991. Water wave mechanics for engineers and scientists. World Scientific , 353.

Fredsoe, J., 1984. Turbulent boundary layer in wave - current motion. Journal of Hydraulic Engineering ASCE 110, 1103–1120.

Ghisalberti, M., Nepf, H.M., 2004. The limited growth of vegetated shear layers. Water Resources Research 40. doi:10.1029/2003WR002776W07502.

Grant, W., Madsen, O., 1979. Combined wave and current interaction with a rough bottom. Journal of Geophysical Research 84(C4), 1979–1808.

Hu, Z., Suzuki, T., Zitman, T., Uittewaal, W., Stive, M., 2014. Laboratory study on wave dissipation by vegetation in combined current - wave flow. Coastal Engineering 88, 131–142.

Jiang, J.Y., Street, R.L., 1991. Modulated flows beneath wind-ruffled, mechanically-generated water waves. Journal of Geophysical Resources 96, 2711–2721.

Jones, C., Lawton, J., Shachak, M., 1994. Organisms as ecosystem engineers. Oikos 69, 373–386.

Kemp, P., Simons, R.R., 1982. The interaction between waves and a turbulent current: waves propagating with the current. Journal of Fluid Mechanics 116, 227–250.

Kemp, P., Simons, R.R., 1983. The interaction between waves and a turbulent current: waves propagating against the current. Journal of Fluid Mechanics 130, 73–89.

Klopman, G., 1994. Vertical structure of the flow due to waves and currents. Tech. rept. H840.32.

Klopman, G., 1997. Secondary circulation of the flow due to waves and current. Tech. rept. Z2249.

Li, C.W., Yan, K., 2007. Numerical investigation of wave - current - vegetation interaction. Journal of Hydraulic Engineering 133-7, 794–803.

Meyer-Peter, E., Muller, R., 1948. Formulas for bed-load transport. Sec. Int. IAHR congress, Stockholm, Sweden .

Musumeci, R., Cavallo, L., Foti, E., Scandura, P., 2006. Waves plus currents crossing at a right angle: experimental investigation. Journal of Geophysical Research 111, C07019.

Nikora, V., Goring, D., McEwan, I., Griffiths, G., 2001. Spatially averaged open - channel flow over rough bed. Journal of Hydraulic Engineering 127(2), 123–133.

Nikora, V., Koll, K., McEwan, I., McLean, S., Dittrich, A., 2004. Velocity distribution in the roughness layer of rough - bed flows. Journal of Hydraulic Engineering 130(10), 1036–1042.

Olabarrieta, M., Medina, R., Castanedo, S., 2010. Effects of wave - current interaction on the current profile. Coastal Engineering 57, 643–655.

Paul, M., Bouma, T., Amos, C., 2010. Wave attenuation by submerged vegetation: com- bining the effect of organism traits and tidal current. Marine Ecology Progress Series 444, 31–41.

Romano, C., Widdows, J., Brinsley, M.D., Staff, F.J., 2003. Impact of enteromorpha intestinalis mats on near-bed currents and sediment dynamics: Flume studies. Marine Ecology Progress Series 256, 63–64.

Shi, Z., Pethick, J.S., Pye, K., 1995. Flow structure in and above the various heights of a saltmarsh canopy: a laboratory flume study. Journal of Coastal Research 11, 1204–1209.

Silva, J.F., Duck, R.W., Catarino, J.B., 2004. Seagrasses and sediment response to changing physical forcing in a coastal lagoon. Hydrology and Earth System Sciences 8, 151–159.

Simons, R., MacIver, R., Saleh, W., 1996. Kinematics and shear stresses from combined waves and longshore currents in the UK coastal research facility. Proceedings of the Coastal Engineering Conference , 3481–3494.

Stephan, U., Gutknecht, D., 2002. Hydraulic resistance of submerged flexible vegetation. Journal of Hydrology 262 (1-2), 27–43. doi:doi:10.1016/S0022-1694(02)00192-0.

Stratigaki, V., Manca, E., Prinos, P., Losada, I., Lara, J., Sclavo, M., Amos, C., Caceres, I., Sanchez-Arcilla, A., 2011. Large scale experiments on wave propagation over posidonia oceanica. Journal of Hydraulic Research 49, 31–43.

Tambroni, N., Blondeaux, P., Vittori, G., 2015. A simple model of wave - current interaction. Journal of Fluid Mechanics 775, 328–348. doi:10.1017/jfm.2015.308.

Thais, L., Magnaudet, J., 1995. A triple decomposition of the fluctuating motion below laboratory wind water waves. Journal of Geophysical Resources 100(C1), 741–755.

Trowbridge, J.H., 1998. On a technique for measurement of turbulent shear stress in the presence of surface waves. Journal of Atmospheric and Oceanic Technology 15, 290–298.

Umeyama, M., 2005. Reynolds stresses and velocity distributions in a wave - current coexisting environment. Journal of Waterway, Port, Coastal and Ocean Engineering 131 (5).

Venier, C., da Silva, J.F., McLelland, S., Duck, R., Lanzoni, S., 2012. Experimental investigation of the impact of macroalgal mats on flow dynamics and sediment stability in shallow tidal areas. Estuarine, Coastal and Shelf Science 112, 52–60. doi:10.1016/j.ecss.2011.12.035.

Visser, P.J., 1986. Wave basin experiments on bottom friction due to currents and waves. Proceedings of the 20th International Conference on Costal Engineering, Taipeh, Taiwan .

Wang, C., Yu, J., Wang, P., Guo, P., 2009. Flow structure of partly vegetated open-channel flows with eelgrass. Journal of Hydrodynamics, Ser. B 21 (3), 301–307. doi:doi:10.1016/S1001-6058(08)60150-X.